Heliyon 10 (2024) e26826

Contents lists available at ScienceDirect

Heliyon

journal homepage: www.cell.com/heliyon

Research article

Dynamic buckling response of buried X70 steel pipe with bolted flange connection under two-charge explosion loads

Yandong Qu [a,*], Ruixue Zhang [b], Jinda Wu [b], Lei Xu [a], Shengnan Zuo [b], Baiyuan Xu [b]

[a] College of Civil Engineering, Dalian Minzu University, Dalian 116650, China
[b] School of Civil and Architectural Engineering, Liaoning University of Technology, Jinzhou 121001, China

ARTICLE INFO

Keywords:
Bolted flange connection
explosion load
buckling response
numerical simulation
X70 pipe

ABSTRACT

It is of great significance to investigate the dynamic response of pipes under blasting loads for the operation, assessment, and repair of pipes. However, there are few studies available on the dynamic buckling response of pipes under multiple explosion loads. In the present study, pipe-soil coupling 3-D models are established to investigate the dynamic buckling response of X70 steel pipe with bolted flange connection (BFC) under two-charge explosion loads (Charge A lied on the ground surface and Charge B lied in the soil). The main influencing factors are also discussed, including explosion mode, internal pressure, interval time, mass ratio of charges, and diameter-to-thickness ratio (D/t ratio). When Charges A and B were exploded simultaneously, it is found that the non-pressurized X70 pipe produced more significant cross-sectional deformation than in one-point explosion (Charge A or B). Increasing D/t ratio is advantageous for the anti-explosion of the pipe with BFC. Suitable internal pressure can effectively prevent the buckling deformation of the pipe. Compared with the common straight pipe, BFC system can effectively decrease the local buckling deformation and improve the anti-explosion ability of the pipe due to its higher local stiffness and energy absorption.

1. Introduction

As one of the main long-transport modes of oil and gas, pipes are normally buried underground due to their larger volume, less influence of weather, simpler operation, and less leakage [1–3]. Bolted flange connection (BFC) and welding connection are the two extensively used modes to connect long-distance transport pipes [4,5]. Many previous studies have presented that BFC can effectively improve the sealing performance and reduce the leakage rate of pipes [6,7]. The studies on the mechanical behavior of pipes with BFC are also getting more attention to ensure the safe operation of the pipes due to intensive construction of urban pipe networks [8–10]. For instance, Hoang et al. [8] experimentally explored the mechanical behavior of high-strength steel pipe with BFC. Chen et al. [9] experimentally investigated the bearing capacity performance of the bolted flange pipes under compression and bending loads. Li et al. [10] presented a new mechanical model of blot connections to reproduce the micro-slip motion between the connection interfaces in flanged cylindrical shell.

With the urbanization speeding up and the densely distributing underground pipe network, pipes are bound to be threatened by explosion attacks and non-human factors exploding [2,11–13], and they have been one of the main reasons for the leakage of pipes. As a sequence, various investigations have been carried out to study the dynamic performance of pipes subjected to explosion load. For

* Corresponding author.
E-mail address: plxfeng2009@sohu.com (Y. Qu).

https://doi.org/10.1016/j.heliyon.2024.e26826
Received 9 February 2023; Received in revised form 16 February 2024; Accepted 20 February 2024
Available online 22 February 2024

Nomenclature

BFC	Bolted flange connection
EOS	Equation of state
σ_y	Yield stress in Eq. (1)
E_s	Elastic modulus in Eq. (1)
E	The strain in Eq. (1)
ε_e	Ultimate elastic strain in Eq. (1)
E_t	Shear modulus in Eq. (1)
P_e	Unit pressure of explosive in Eq. (2)
P_{eos}	Pressure of EOS in Eq. (2)
V	Relative volume in Eq. (2)
E	Initial internal energy per unit volume of explosive in Eq. (2)
A, B, ω, R_1, R_2	The five constants of explosive material in Eq. (3)
P_A	The pressure
E_i	Initial internal energy density in Eq. (3)
S_{ij}	Cauchy deviator stress tensor in Eq. (4)
δ_{ij}	Kronecker coefficient in Eq. (4)
a_0	Friction angle of soil in Eq. (4)
a_1	Force of cohesion in Eq. (4)
a_2	Influence coefficient of explosion effect in Eq. (4)
P	Pressure of soil in Eq. (4)
μ	Particle displacement in Eq. (5)
μ	The function of the density ρ, and reference density ρ_0 in Eq. (5)
$C_{0\text{-}6}$	The coefficients of EOS in Eq. (5)
D	Outer diameter of pipe in Eq. (6)
$\triangle D$	The amount of outer diameter of the pipe in Eq. (6)
σ	Combined stress of axial stress and circumferential stress in Eq. (7)
ρ	Density of soil in Eq. (7)
υ	Peak vibration velocity in Eq. (7)
t	Interval time in Eq. (7)
P_i	Internal pressure in Eq. (7)
C	Vibration velocity of particle in Eq. (7)
H	Distance from blasting center to the particle of pipe in Eq. (7)
δ	Pipe wall thickness in Eq. (7)
Q	Explosive mass in Eq. (7)
χ	Particle displacement in Eq. (7)
$\alpha_{1\text{-}5}$	The five coefficients in Eq (12)
k	Influence coefficient of test site in Eq. (13)
$\beta_{1\text{-}5}$	The five coefficients in Eq. (13)

instance, Qu et al. [2] numerically predicted the dynamic behavior of buried polyethylene (PE) pipe under single point explosion for the first time. Moreover, parametric studies are also carried out to show the dynamic response of the PE pipes subjected to subsurface localized explosion [2]. Wu et al. [14] discussed the influence of different explosion parameters and pipe parameters on the peak stress of buried pipes under ground surface explosion. Mokhtari et al. [15] investigated the influence of diameter-thickness ratio (D/t ratio) of pipe and internal pressure on the dynamic performance of the pipe under single-point blast load. He et al. [16] numerically investigated the influence of the size of an explosive and pipe parameters on the damage of pipe caused by large explosives. Parviz et al. [17] studied the parameters of pipes buried in two soil types under explosion load. They presented that the greater the soil density, the greater the pressure and stress transfer of the pipes.

Explosion test is the most intuitive and effective method to explore the anti-explosion performance of the structures [18]. However, it is easily affected due to the test conditions of external geology, the high cost of the test, and the high accuracy of the test equipment. With the development of computer technology, numerical studies have been extensively carried out to the dynamic characteristics of buried pipes under explosion loads [19–24]. For instance, Lu and his coworkers established a multiphase coupled model of pipe, soil and fluid within the pipe to describe structural dynamic response of buried pipe subjected to external explosion load [20]. Zhang and his coworkers [21] numerically investigated the dynamic buckling properties of ordinary steel pipes under multi-point explosion loads. Zhao et al. [22] numerically studied the dynamic failure mechanism of gas pipes with flange joint under explosion load. Ji et al. [23] numerically studied the influence of vibration-isolating slot on buried pipes under blast loading. They pointed out that the vibration speed of the pipe could be decreased. An et al. [24] numerically investigated the dynamic response of buried PE100 gas pipes containing a scratch defect under impact load of collapsed body.

At present, numerical method has been one of the useful supplement methods and accepted by more and more researchers [25–30]. Many previous studies have shown that it can simulate the propagation law of shock waves and their impact on the dynamic response of various structures, such as slabs [26,27], beams [28], bridge decks [29], and pipes [30,31]. As far as the pipes were consented, most of the researchers concentrated their efforts on studying the dynamic performance of pipes under single-point explosion load [13–18, 30,31]. However, multiple explosions often occur in actual terrorist attacks or industrial demolition [32,33]. Multiple initiation and simultaneous explosion of multiple charges could result in greater damage and loss to personnel and property due to the superposition of shock waves under certain conditions. Compared with single-point explosion, the propagation law of shock waves are more complex in the two-point and multiple explosion loads. As a sequence, in recent years, many scholars have carried out extensive and in-depth studies on the effect of multiple explosions [34–36]. For instance, Wang et al. [34] numerically investigated the damage evolution characteristics of the bolt-supported cavern subjected to multiple explosions. Bai et al. [35] investigated the characteristics of blast loads formed from the two simultaneous detonated explosive charges in real air. Huang et al. [36] numerically investigated the dynamic response of brain under single and repetitive blast waves by using Euler–Lagrange coupling method.

In conclusion, the dynamic properties of pipes under blast loads have been widely studied, especially under single-point explosion load as mentioned above. However, there are few reports on the dynamic buckling response analysis of buried pipes with BFC under explosion loads. As a sequence, it is numerically investigated to study the dynamic buckling behavior of the buried X70 steel pipe with BFC under multiple explosion loads by using nonlinear finite element (FE) code ANASYS/LS-DYNA. The main influencing factors are also discussed, including explosion mode, internal pressure, interval time, mass ratio of charges, and diameter-to-thickness ratio (D/t ratio). Moreover, BFC could effectively decrease the local buckling deformation of the pipe with BFC under two-charge explosion loads due to the local increasing stiffness of the pipe and energy absorption of gaskets. The buckling response analysis of the pipe with BFC was the emphasis of present study and the two charges (Charge A and B) facing the pipes were placed away from the flange plates. Dimensional analysis extensively used to deal with the dynamic influencing factors in the blasting response study [37,38], was also used to establish the stress prediction model and analyze the loading standard of the pipes under multiple explosion loads.

2. FE modeling and material models

2.1. Material models

Various nonlinear material models and equation of state (EOS) are used to model the dynamic behavior of materials involved in the problem, namely X70 steel, soil, explosive, air, flange, gasket, and bolt. The material models and EOS are concisely explained in the following.

2.1.1. Material model for X70 steel

The kinematic hardening material model (MAT_PLASTIC_KINEMATIC) is used to simulate isotropic rigid plastic materials of the X70 steel pipe with BFC. This model follows Von misses yield law, and the stress-strain relationship is expressed as Eq. (1) [12,30]:

$$\sigma = \begin{cases} E_s\varepsilon & \varepsilon \le \varepsilon_e \\ \sigma_y + E_t(\varepsilon - \varepsilon_e) & \varepsilon > \varepsilon_e \end{cases} \tag{1}$$

Where σ_y is the yield stress; E_s is the elastic modulus; E_t is the shear modulus; ε is the strain; ε_e is the ultimate elastic strain. Table 1 presents material constants of X70 steel [12,30].

2.1.2. Material model for explosive

Explosive charges is modelled by using the high-energy explosion model (MAT_HIGH_EXPLOSIVE_BURN). Explosive explosions could result in the release energy and the pressure of nearby materials is changed. In the simulation, the explosive unit pressure is expressed as Eq. (2) [39,40]:

$$P_e = FP_{eos}(V, E) \tag{2}$$

Where P_{eos} is the pressure of EOS; V is the relative volume; and E is the initial internal energy per unit volume of explosive.

The pressure generated by the expansion of the detonation products of the explosive is described by the JWL equation [39,40]. It is shown in Eq. (3):

Table 1
Material constants of X70 steel [12,30].

Material properties	X70 steel
Density (g/cm^3)	7.93
Possion's ratio	0.3
Young's modulus (GPa)	210
Yield stress (MPa)	480

$$P_{eos} = A\left(1 - \frac{\omega}{R_1 V}\right)e^{-R_1 V} + B\left(1 - \frac{\omega}{R_2 V}\right)e^{-R_2 V} + \frac{\omega E}{V} \tag{3}$$

where, R_1、R_2、A、B and ω are the constants of the material; V is the relative volume; E is the internal energy per unit volume. The material parameters of TNT charge are listed in Table 2 [12,30].

2.1.3. Material model for soil

The material model of MAT_SOIL_AND_FOAM is used to define the loess soil in the experimental site, and its yield equation is expressed as Eq. (4) [41]:

$$\varphi = S_{ij}\delta_{ij} / 2 - \left(a_0 + a_1 P + a_2 P^2\right) \tag{4}$$

Where S_{ij} and δ_{ij} are the Cauchy deviator stress tensor and Kronecker coefficient, respectively; a_0~a_2 are the coefficients of friction, cohesion, and explosion effect of the soil, P is the pressure of the soil. Table 3 illustrated the material constants of soil [12,30,42].

2.1.4. Material model for air

The material model (MAT_NULL) and the polynomial equation are used to define air. This is shown in Eq. (5) [12,30]:

$$P = C_0 + C_1\mu + C_2\mu^2 + C_3\mu^3 + \left(C_4 + C_5\mu + C_6\mu^2\right)E \tag{5}$$

Where P is the pressure; E_i is the initial internal energy density; μ is the function of the density ρ, and the reference density ρ_0; C_0 to C_6 is the seven coefficients of EOS. The material parameters of air [12,30] are listed in Table 4.

2.1.5. Material models for flange, gasket, and bolt

The material model (MAT-PLASTIC-KINE-MATIC) is used to define the flange, which is made of 316L austenitic stainless steel (00Cc17Ni14M02). Moreover, it is also used to define spiral material, which is made of 35CrMoA alloy steel. The material model (MAT-BLATA-KO-RUBBER) is used to define the gasket, which is made of polyurethane rubber. The material parameters of flange, gasket, and bolt are listed in Table 5 [43].

2.2. Dimensions, meshing and general settings

Fig. 1 shows the structural diagram of one part (cross-section) of the X70 steel pipe with BFC, which is composed of the pipe, flanges, gaskets and bolts. The calculation model is shown in Fig. 2 by using commercial code ANSYS/LS-DYNA [44]. The whole model is 310 cm × 250 cm × 191.9 cm in the x-, y-, and z-directions (See Fig. 2). Charge A lied on the ground surface is a rectangle (TNT explosive), having dimensions 24 cm × 40 cm × 20 cm, and Charge B is a rectangle in soil, which has dimensions 20 cm × 12 cm × 16 cm. The burial depth of Charge B is 82.65 cm. The outer diameter of the pipe is 81.3 cm and the thickness of pipe wall is 1 cm according to the National Standardization Administration of China [45,46].

The detail information of the pipe with BFC is shown in Table 6. SOLID164 is used for the 3-D model of solid structures in the development of numerical models. The element is defined by 8 nodes. Each node has the degrees of freedom as follows: translations, velocities, and accelerations in the x-, y-, and z-directions. The explosive charges and soil are connected by Arbitrary Lagrange-Euler (ALE) algorithm.

The top surface of ground is defined by using a free boundary shown in Fig. 2. The non-reflecting boundary conditions are used to define boundary conditions of soil shown in Fig. 2. The displacement constraints are applied on both ends of the pipe. Meshing of air, TNT and soil is illustrated in Fig. 3(a). Moreover, meshing of the X70 pipe with BFC is illustrated in Fig. 3(b).

It is well known that the grid size directly affects the calculation time and simulation accuracy. As a sequence, many studies have analyzed the mesh density sensitivity to structural dynamic response under explosion loads [46–48]. In the present study, suitable mesh size of the X70 pipe with BFC is 0.12–2.50 cm, and grid encryption is performed in the vicinity of the flange dish. The mesh size of the soil and explosive model is 1.7–4.0 cm to ensure the accuracy of the simulation results. The grid size of the present study is reasonable on the conditions of considering the limitations of computer simulation conditions and calculation time. The contact is

Table 2
Material parameters of TNT charge [12,30].

Material properties	Value
Density (g/cm^3)	1.64
Detonation velocity (m/s)	6930
C-J pressure (GPa)	27
A(GPa)	0.374
B(GPa)	0.00323
R_1	4.15
R_2	0.95
ω	0.3
E_i(J/m^3)	7×10^9

Table 3
Material constants of soil [12,30,42].

Material properties	Soil
Density (g/cm^3)	1.80
Shear modulus (GPa)	0.04114
Bulk modulus (MPa)	87.87
A_0 (10^8 Pa^2)	2.12
A_1 (10^3 Pa)	5.23
A_2 (10^{-2})	3.22

Table 4
Material constants of air [12,30].

Material properties	air
Density (g/cm^3)	0.0012929
C_0	0
C_1	0
C_2	0
C_3	0
C_4	0.4
C_5	0.4
C_6	0

Table 5
Material constants of flange, gasket, and bolt [43].

Material properties	Flange	Gasket	Bolt
Density (g/cm^3)	7.86	1.21	7.86
Passion' s ratio	0.28	0.463	0.3
Young's modulus (GPa)	200		202
Shear modulus (GPa)		0.00267	
Yield stress (MPa)	180		740

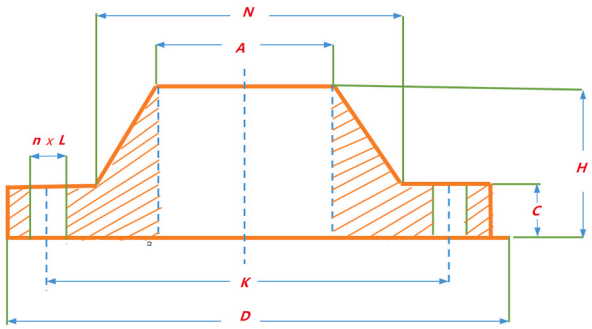

Fig. 1. Structural diagram of one part (cross-section) of X70 steel pipe with BFC.

created between Lagrangian mesh surfaces (soil) and Eulerian material surfaces (pipe) by using a penalty contact algorithm [12,30]. *INITIAL_DETONATION is extensively used to define detonation point and initiation time. Considering the very short loading duration, time step is crucial for the validity of the numerical results. The time step size roughly corresponds to the transient time of an acoustic wave through an element using the shortest characteristic distance in the commercial software ANSYS/LS-DYNA [2,44]. The detail information about time step and *INITIAL_DETONATION could refer to the relevant references [2,44].

In the present study, the following two hypotheses are also put forward to simplify the research problem.

(1) The self-weight of the X70 steel pipe with BFC was not considered during the total explosion process.
(2) The leakage performance and fracture failure of bolts are also not considered.

3. Orthogonal test

Larger-diameter pipes are chosen to study the dynamic buckling behavior of the buried X70 pipe with BFC under two-charge

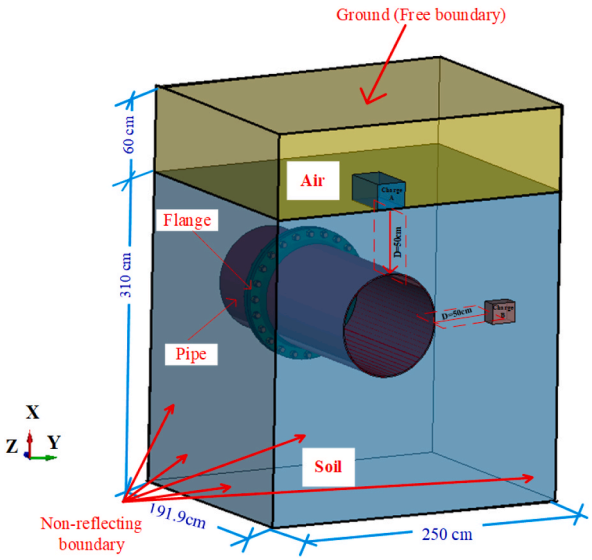

Fig. 2. Calculation model.

Table 6
The detail information of X70 steel pipe with BFC [42,46].

Nominal size DN	800
Outer diameter of the flange welding end of steel pipe A/mm	813
Flange outer diameter D/mm (Connection size)	1025
Center circle diameter of bolt hole K/mm (Connection size)	950
Bolt diameter L/mm (Connection size)	39
Bolt amount (Connection size)	24
Bolt thread Specification (Connection size)	M36
Flange thickness C/mm	41
Flange hight H/mm	108
Flange neck N/mm	855

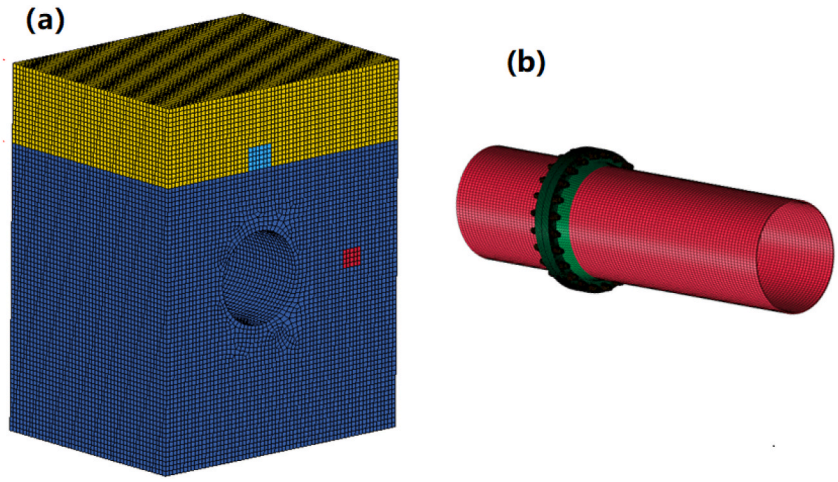

Fig. 3. Meshing of calculation model: (a) meshing of air, TNT charges and soil; (b) meshing of the X70 pipe with BFC.

explosion loads. The main four influencing factors are considered as follows: explosive charge (Q), internal pressure of pipe (P_i), pipe radius (R), and interval time (t). Numerical simulation test is designed on the basis of the influencing factors mentioned above. Table 7 shows the horizontal values of each influencing factor.

Table 7
Horizontal values of each influencing factor.

	Influencing factors			
	t/μs	Q/kg	P_i/MPa	R/cm
Case 1	0	6.298	0	20.35
Case 2	300	8.387	2	22.60
Case 3	600	13.120	4	29.05
Case 4	900	18.893	6	40.65
Case 5	1200	31.488	8	50.80
Case 6	1500	–	–	–

4. Numerical results and discussion

4.1. Flatness coefficient analysis

Since the closed high-rate explosive explosion could result in the reduction of content flow, the pipe section may have larger deformation [13]. The amount of cross-sectional deformation of the pipe with BFC is also determined by "flattening parameter" f, which is defined as Eq. (6) [49]:

$$f = \frac{\Delta D}{D} \tag{6}$$

Where D is the outer diameter of the pipe, and $\triangle D$ is the amount of outer diameter of the pipe. The cross-sectional flattening par state occurs when the parameter f exceeds 0.15 [49].

Fig. 4 shows the changing trend of flattening parameter values of the non-pressurized X70 steel pipe with BFC under a single point and multiple explosion loads. After Charge A was exploded on the ground surface, f was still 0 at 1000 μs (See Fig. 4). With the propagation time increasing, f was significantly increased and it got a maximum value at about 1250 μs, which was less than 0.15. Finally, f was further increased with the time further increasing after 1500 μs. The slope of the horizontal parameter-time curves had leveled off. However, when Charge B was exploded or the two charges were exploded simultaneously shown in Fig. 4, the similar phenomena was not observed during the explosion process. Meanwhile, when Charge B was exploded in the soil, f was less than 0.15. Charge A and Charge B exploded simultaneously could result in the increasing of the flattening parameter value, and it exceeded 0.6, which was more than its critical value.

In conclusion, BFC could effectively decrease the local deformation of the X70 steel pipe under two-charge explosion loads due to the local increasing stiffness of the pipe and energy absorption of gaskets.

4.2. Dynamic response analysis

4.2.1. Influence of explosion modes

Fig. 5 shows the influence of explosion modes on the effective stress of the non-pressurized X70 steel pipe with BFC over the period of detonation. When Charge A was exploded on the ground surface, the maximum effective stress value of 480.2 MPa could be found

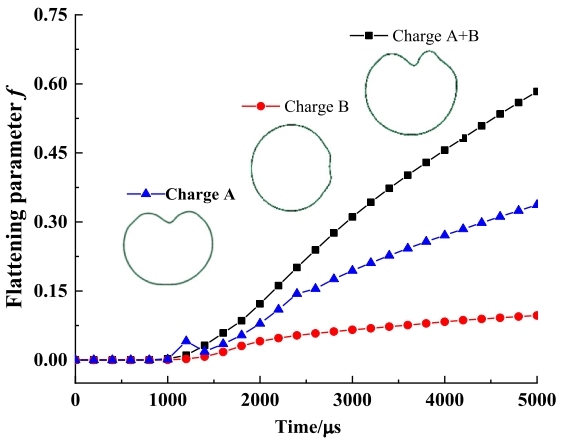

Fig. 4. Flattening parameter values of the non-pressurized X70 steel pipe with BFC (Charge A lied on the ground surface, Charge B lied in the soil, and Charge A + B means Charge A and Charge B were exploded simultaneously).

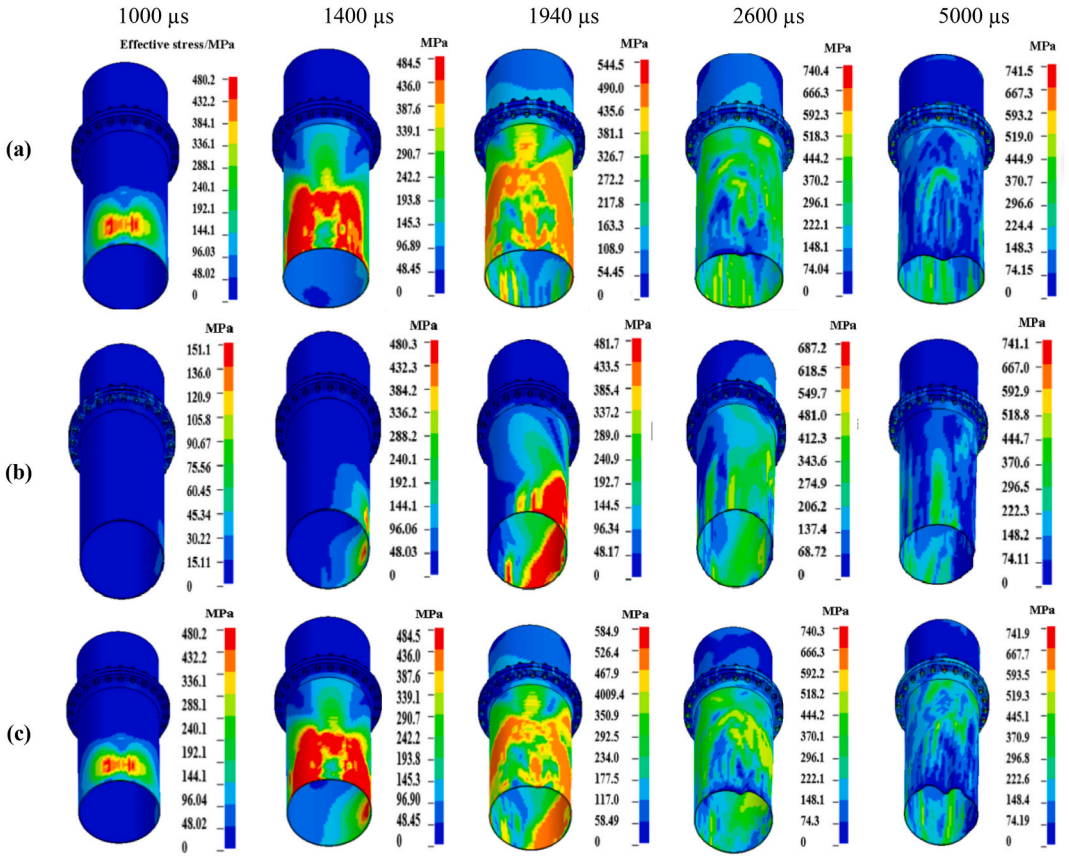

Fig. 5. Influence of explosion modes on the effective stress of the non-pressurized X70 pipe with BFC: (a) Charge A; (b) Charge B; (c) Charge A + B.

exactly beneath Charge A shown in Fig. 5(a) at 1000 μs. Then, the deformation of the pipe was increased with the propagation time increasing. The maximum effective stress is also increased. The location of maximum equivalent stress moves along the pipe, and goes farther from the location of the pipe facing the charge (See Fig. 5(a)). When Charge B was exploded in the soil, the maximum equivalent stress of the same pipe with BFC was relatively smaller at the same propagation time (See Fig. 5(b)).

For instance, the peak effective stress of the pipe for Charge B is less 53.2 MPa than that of the same pipe for Charge A at 3600 μs. The peak effective stress is almost equal for the three explosion modes at 5000 μs. The bolts could get the maximum effective stress due to the absorption of the shock waves' energy. As a sequence, BFC can effectively decrease the local deformation of the pipe under two-charge explosion loads due to the local increasing stiffness and energy absorption of bolts.

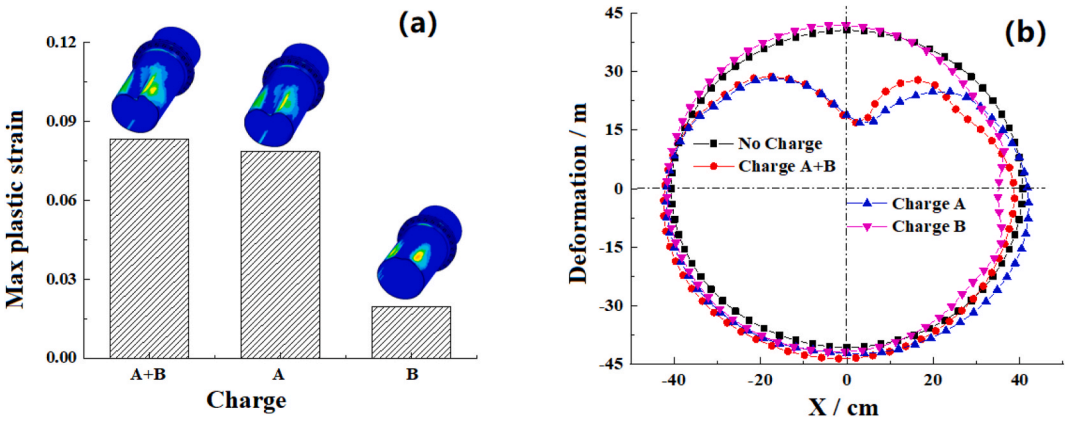

Fig. 6. Influence of explosion modes on the maximum plastic strain (a) and the cross-sectional deformation (b) of the non-pressurized X70 pipe with BFC (Charge A + B means the two charges were exploded simultaneously).

Fig. 6 shows the influence of explosion modes on the maximum plastic strain and the cross-sectional deformation of the non-pressurized X70 pipe with BFC. When Charge A and Charge B were exploded simultaneously, the maximum plastic strain and significant cross-sectional deformation were formed above the pipe and the right side of the pipe facing the charge center (See Fig. 6(a and b)). The maximum plastic strain of the pipe for Charge A is almost 4 times than that of the same pipe for Charge B. The maximum plastic strain of the pipe for Charge A + B is smaller than that of the same pipe for Charge A. The cross-sectional deformation of the pipe is mainly composed of four parts as follows: the larger dent on the upside, the smaller dent on the right side of the pipe, and ovalization on the left side and bottom of the pipe (See Fig. 6(b)). As can be seen from Fig. 6, when Charge B was exploded in the soil, the deformation of the X70 pipe is relatively small, and a minor depression was generated on its right side. The dent position lies on the right side of the pipe for Charge B, which is different from Charge A + B. The pipe got the minimal plastic strain because part of the shock waves was absorbed by the surrounding soil of the charge. Moreover, BFC can effectively decrease the local buckling deformation of the pipe under two-charge explosion loads due to the local increasing stiffness of the pipe and energy absorption of the bolts.

4.2.2. *Effect of internal pressure*

Fig. 7 shows the influence of internal pressures on the effective stress of the pressurized pipe under two-charge explosion loads. When Charges A and B were simultaneously exploded, the effective stress was concentrated on the extended pipe portion of the pipe (See Fig. 7). A significant collapse deformation lied on the underneath of the pipe (away from BFC) shown in Fig. 7 (a). As the internal pressure increases, the effective stress is axially distributed along the pipe shown in Fig. 7(b–e).

Fig. 8 shows the influence of internal pressures on the maximum plastic strain and the cross-sectional deformation of the pressurized pipe under two-charge explosion loads (Charge A + B). When the internal pressure reached 4 MPa, the produced plastic strain was minimized (See Fig. 8(a)). When it is greater than 4 MPa, the influence of internal pressure is lowered. When the internal pressure is 0, larger cross-sectional deformation of the pipe can be easily observed (See Fig. 8(b). The collapse deformation of the pipe is lowered with the increasing of internal pressure, and the variation amount of displacement is smaller. As a sequence, it is concluded that suitable internal pressure can effectively prevent the buckling deformation of the pipe under two-charge explosion loads.

4.2.3. *Influence of interval time*

Fig. 9 shows the influence of interval time on the effective stress of the X70 pipe with BFC under two-charge explosion loads (mass-constant Charge A was located on the ground typically explosion, and changing the mass of charge B located in the soil shown in Table 4). It is obvious that changing internal time has little effect on the peak effective stress of the pipe with BFC under the two-charge explosion loads (See Fig. 9). The generated region of higher effective stress is broader along the axial direction of the pipe. The stress concentration was also gradually apparent. As the interval time was increased, the depression angle above the pipe gradually increased.

Fig. 10 shows the maximum plastic strain and the maximum cross-sectional deformation of the pipe with BFC under two-charge explosion loads at different interval times. Compared with the straight pipes under multiple explosion loads [29], the variation of plastic strain of the pipe with BFC is smaller at the same interval time. The plastic strain values of the pipe were maximized at two points (See Fig. 10(a)). The transverse collapse deformation of the cross-section of the pipe with BFC lied on the upper portion and the upper right of the pipe shown in Fig. 10 (b). When the interval time is 300 μs, the upper top exhibits a concave shape and the interval time is gradually increased.

4.2.4. *Effect of mass ratio of charge A and charge B*

In the present study, the mass of Charge A is fixed and the amount of Charge B is changed to explore the influence of the mass ratio of Charge A and Charge B (Charge A/B) on the effective stress of the pipe. With the increase of the mass ratio of Charge A/B from 1.0 to 5.0, the maximum effective stress of the pipe is reduced from 750.3 to 741.4 MPa (See Fig. 11).

Fig. 12 shows the influence of mass ratio of Charge A/B on the maximum plastic strain and the cross-sectional deformation of the pipe under two-charge explosion loads. With the mass ratio of Charge A/B increasing, the maximum plastic strain of the pipe with BFC

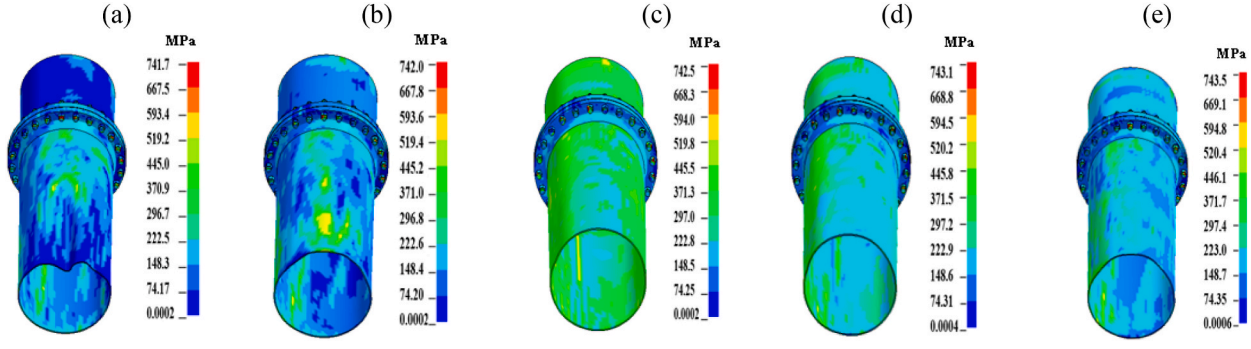

Fig. 7. Influence of internal pressures on the effective stress of the pressurized pipe under two-charge explosion loads: (a) 0 MPa; (b) 2 MPa; (c) 4 MPa; (d) 6 MPa; (e) 8 MPa.

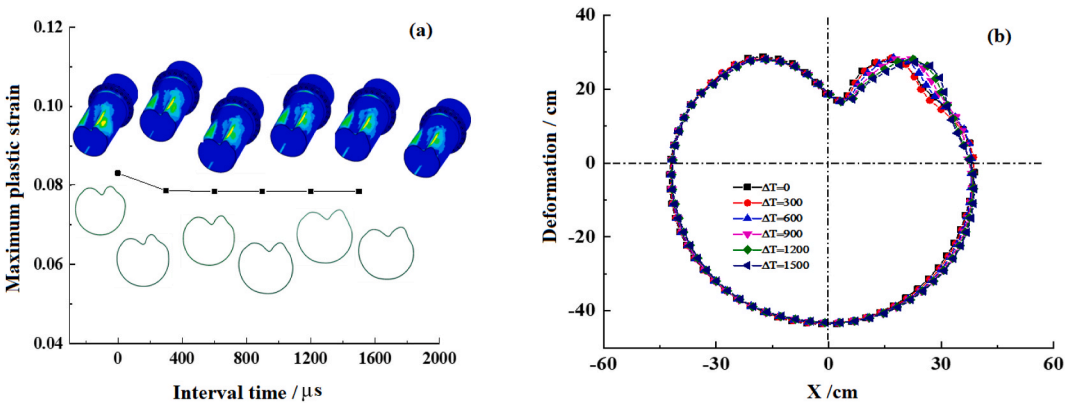

Fig. 8. Influence of internal pressure on the maximum plastic strain: (a) and the cross-sectional deformation of the pipe (b) under two-charge explosion loads.

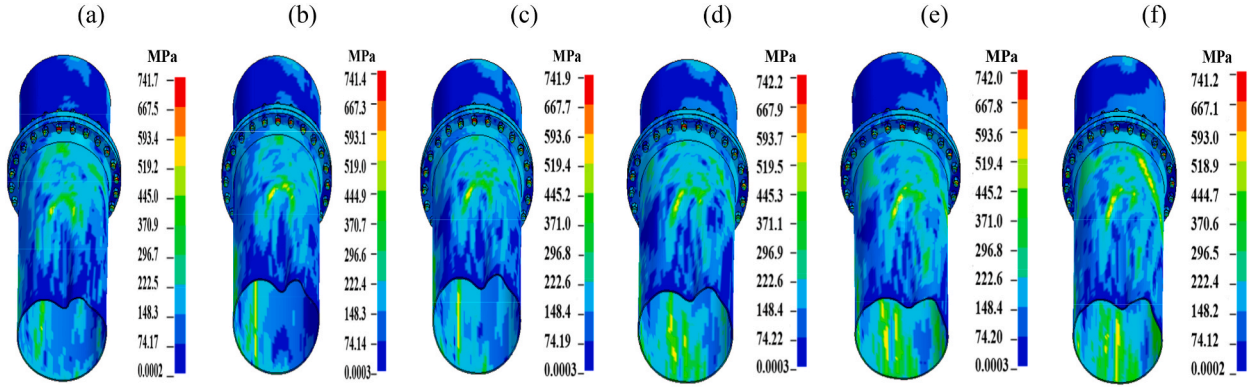

Fig. 9. Influence of interval time on the effective stress of the X70 steel pipe with BFC under two-charge explosion loads.

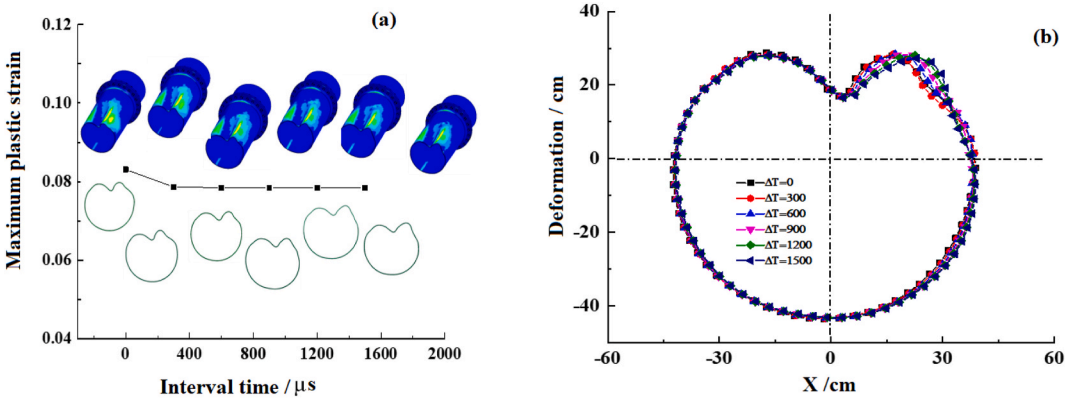

Fig. 10. The maximum plastic strain and maximum cross-sectional deformation of the pipe with BFC under two-charge explosion loads at different interval times.

is quickly reduced, and the changing trend is slowly reduced. For instance, when the mass ratio of Charge A/B is 1.00, the maximum plastic strain of the pipe is 0.2339. When the mass ratio of Charge A/B is 1.67, the maximum plastic strain of the pipe is rapidly more minor to 0.1171(See Fig. 12(a and b)). However, when the mass ratio of Charge A/B is more significant than 1.67, the plastic strain regions on the right side of the pipe gradually disappeared.

In conclusion, BFC could effectively decrease the influence of the mass ratio of Charge A/B, which could also result in the local buckling deformation of the pipe due to the local increasing stiffness of the pipe and energy absorption of gaskets.

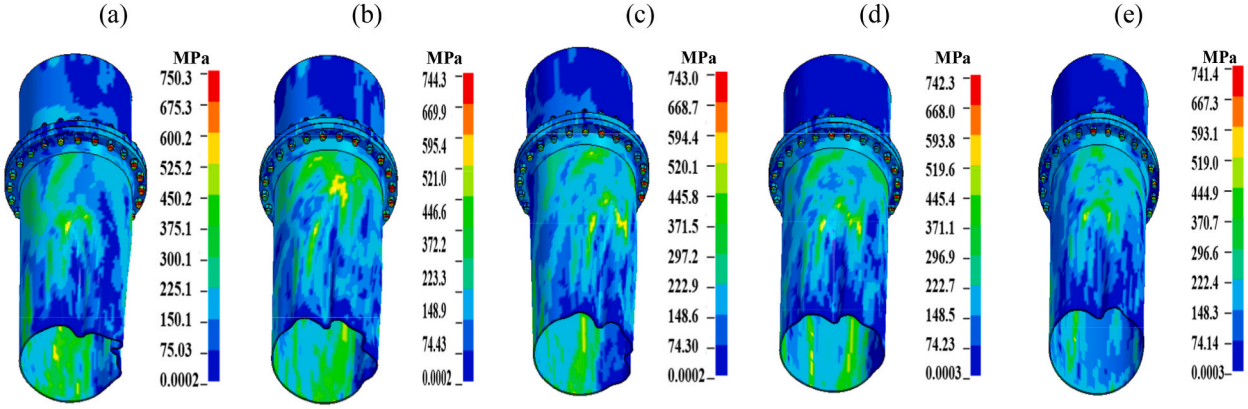

Fig. 11. Influence of mass ratio of Charge A and Charge B on the effective stress of the pipe with BFC under two-charge explosion loads.

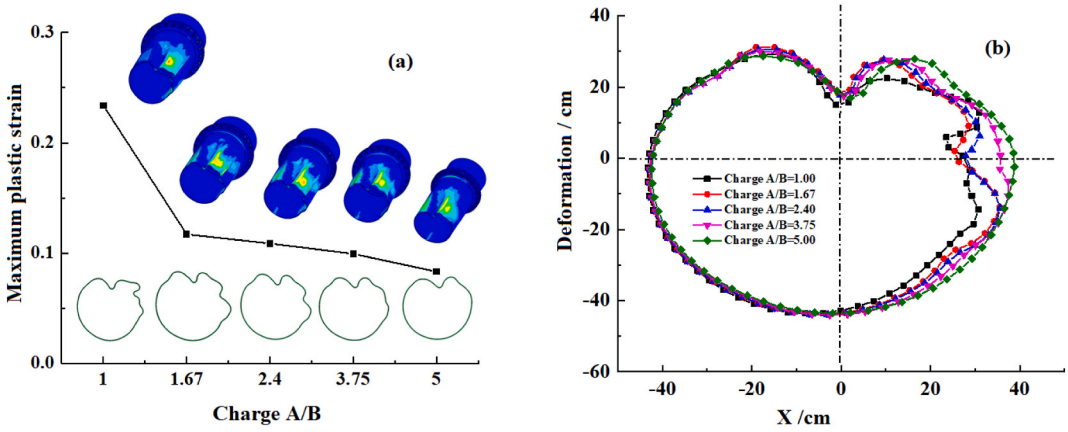

Fig. 12. Influence of mass ratio of Charge A/B on the maximum plastic strain and the cross-sectional deformation of the pipe under two-charge explosion loads.

4.2.5. Effect of D/t ratio

Fig. 13(a–e) shows the influence of the D/t ratio on the effective stress of the X70 pipe under multiple explosion loads. When the D/t ratio of the pipe is 101.6 (See Fig. 13(e)), the maximum effective stress is concentrated on the long pipe end, near the bolted flange system, and the distribution of the effective stress of the short pipe portion is small shown in Fig. 13(e). The reduction of the D/t ratio of the pipe could effectively reduce the axial length of the deformation zone of the pipe (Fig. 13(d)).

Fig. 14 shows the influence of D/t ratio on the maximum plastic strain and the cross-sectional deformation of the pipe under two-charge explosion loads. As shown in Fig. 14 (a), when increasing D/t ratio of the pipe with BFC from 40.7 to 81.3, the maximum plastic strain of the pipe has limited changes. When D/t ratio of the pipe is more than 81.3, the maximum plastic strain of the pipe increased greatly. Moreover, when the pipe has a diameter ratio of 101.6, the collapse displacement of the pipe is the largest, and the upper portion and the right side of the pipe have a concave-shaped deformation shown in Fig. 14 (b). When the pipe has a D/t ratio of 45.7, the upper portion of the conduit generates a projection, and the upper portion of the conduit in the other four working conditions has a concave-shaped deformation. The results show that the larger diameter-thickness ratio is more susceptible to the damage of the explosion shock wave. Suitable for use in the actual reach of the project, increasing the diameter-thickness ratio is advantageous for the use of pipe with BFC.

To sum up, the main four influencing factors are discussed to investigate the influence of initiation points, internal pressure, interval time, explosive mass, and D/t ratio on the dynamic buckling response of the pipe with BFC. However, there is a certain correlation between the above influencing factors. In order to further explore this correlation, the following section will discuss on how to obtain the stress prediction formula, establish the stress prediction model, and analyze the loading standard of pipe under two-charge explosion loads to prevent damage by dimensional analysis.

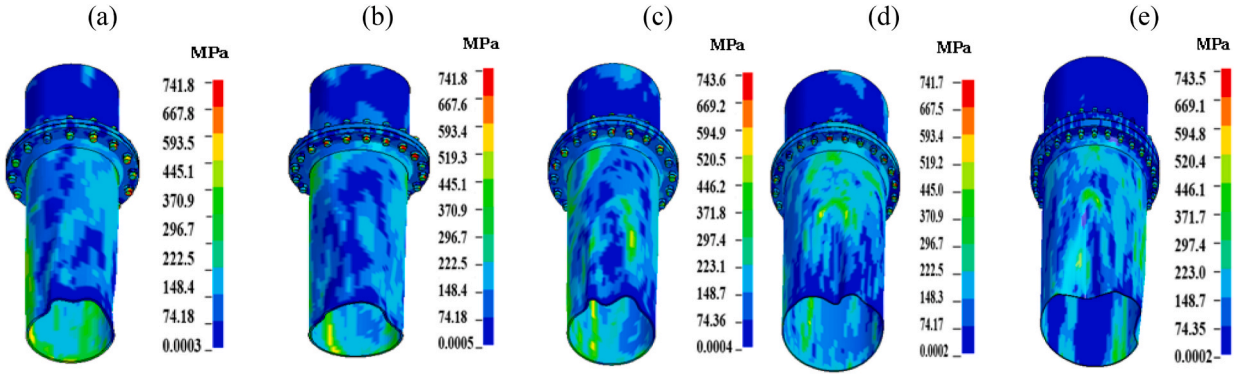

Fig. 13. Influence of D/t ratio on the effective stress of the pipe under two-charge explosion loads: (a) 40.64; (b) 45.7; (c) 50.8; (d) 80.3; (e) 101.6.

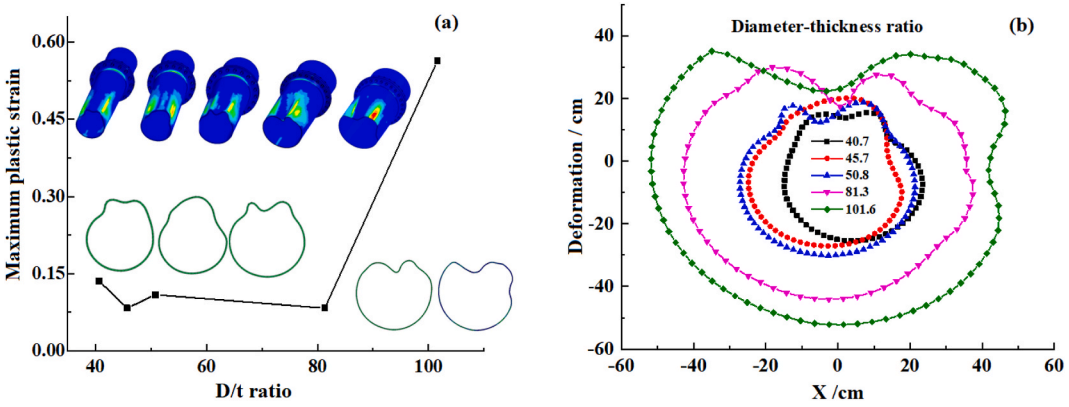

Fig. 14. Influence of D/t ratio on the maximum plastic strain (a) and the cross-sectional deformation (b) of the pipe under two-charge explosion loads.

5. Stress prediction model and control measures analysis

5.1. Stress prediction model

Dimensional analysis of Golden Han Treatment was used to predict the stress of buried pipes under blasting loads. The parameters including the distance from the pipes to blasting center, the physical and mechanical parameters, the properties of explosive, soil medium, blasting parameters can result in the changes of attenuation law of explosion waves. Therefore, ten physical quantities caused the stress changes of pipe can be extracted by reviewing the analysis of the literature and the variation of blasting effect as follows: vibration peak speed v, m/s; interval time t, s; internal pressure P_i, g/cm·μ^2; vibration speed C, m/s; distance from the center point to the position of the pipe H, m; pipe wall thickness δ, m; explosives Q, kg; soil density ρ, kg/m^3; pipe diameter D, m; particle displacement χ, m. From these ten reference physical quantities, three factors of the independent basic dimensions are selected in the present study.

The stress component of the pipe can be shown in Eq. (7) as follows:

$$\sigma = \mathrm{f}(v, t, P_i, C, H, \delta, Q, \rho, D, \chi) \tag{7}$$

It can be seen from the π-theorem that the physical quantity of the studies can be combined into the equivalent equation, as shown in Eq. (8):

$$\pi = Q^x H^y C^z \tag{8}$$

That is, the basic amount selected from the other physical quantity is sequentially shown in Eq. (9):

$$\pi_1 = \frac{V}{C};\ \pi_2 = \frac{t}{HC^{-1}};\ \pi_3 = \frac{P_i}{QH^{-3}C^2};\ \pi_4 = \frac{\delta}{H};\ \pi_5 = \frac{\rho}{QH^{-3}};\ \pi_6 = \frac{D}{H};\ \pi_7 = \frac{\chi}{H} \tag{9}$$

According to the dimensional characteristics, the combination of different dimensions is still one corresponding amount, and π_3, π_6, and π_7 can be extracted to create a new amount of item π_8, as shown in Eq. (10):

$$\pi_8 = (\pi_2)^{\beta_2}(\pi_3)^{\beta_3}(\pi_5)^{\beta_5}(\pi_6)^{\beta_6}(\pi_7)^{\beta_7} = \left(\frac{t}{HC^{-1}}\right)^{\beta_2}\left(\frac{p_i}{QH^{-3}C^2}\right)^{\beta_3}\left(\frac{\rho}{QH^{-3}}\right)^{\beta_5}\left(\frac{D}{H}\right)^{\beta_6}\left(\frac{\chi}{H}\right)^{\beta_7} \tag{10}$$

As a sequence, Eq. (10) can be expressed as Eq. (11):

$$\sigma = f\left(\frac{t}{H}, \frac{P_i}{H}, \frac{\sqrt[3]{\rho}H}{\sqrt[3]{Q}}, \frac{D}{H}, \frac{\chi}{H}\right) \tag{11}$$

Since the medium material is the same and the measurement points are fixed, ρ and C, χ are considered as constants, and β_3, β_6, and β_7 are the corrected factors associated with blasting operations. Combined with the definition of other pending coefficients, the numbers are taken on both sides and a new functional relationship could be obtained shown in Eq. (12):

$$\ln\sigma = \left[\alpha_1 + \beta_1 \ln\left(\frac{t}{H}\right)\right] + \left[\alpha_2 + \beta_2 \ln\left(\frac{P_i}{H}\right)\right] + \left[\alpha_3 + \beta_3 \ln\left(\frac{\sqrt[3]{Q}}{H}\right)\right] + \left[\alpha_4 + \beta_4 \ln\left(\frac{D}{H}\right)\right] + \left[\alpha_5 + \beta_5 \ln\left(\frac{1}{H}\right)\right] \tag{12}$$

Where α_1, α_2, α_3, $\alpha 4$, and α_5 are given during the function transformation process. The established a new predictive mathematical model of stress of the pipe under flat terrain condition is expressed as Eq. (13):

$$\sigma = k(t)^{\beta_1}(P_i)^{\beta_2}\left(\sqrt{3Q}\right)^{\beta_3}(D)^{\beta_4}(H)^{\beta_5} \tag{13}$$

Where k represents the influencing coefficient of test site, β_1 represents the influencing coefficient of the interval of the two-charge explosions on the peak stress of the pipe; β_2 represents the influencing coefficient of internal pressure on the peak intensity of shock waves; β_3 is the influencing coefficient of shock waves on its peak intensity; β_4 the influencing coefficient of blasting distance on the peak intensity of shock waves; β_5 represents the influencing coefficient of the pipe diameter on the peak intensity of shock waves.

The orthogonal test data of Table 7 were analyzed in combination with the results of the above-described correlation analysis and Buckingham theorem (π theorem), including t, Q, P_i, R, as shown in Table 8.

5.2. Control measures analysis

It is of great significance to investigate the control measures of pipes under blasting loads for the operation, assessment, and repair of pipes. Fig. 15 shows the pipe diameter-explosive charge curves of the X70 pipe with BFC under two-charge explosion loads at different propagation times. When Charge A is fixed to 31.488 kg, the following data analysis of Charge B is performed shown in Table 7. As can be seen from Fig. 15(a), the influence of internal pressure on the dynamic response of the pipe is greater than that of inner diameter of the pipe at 300 μs. Meanwhile, compared with the mass of charge, the internal pressure of the pipe has more significant influence on the buckling response of the pipes with BFC. For instance, when the internal pressure exceeds 2 MPa, the internal pressure could weaken the action of the external shock waves on the pipes (See Fig. 15(b–d)). More importantly, when the bural depth of the pipe is fixed to 50 cm, the more increasing D/t ratio of the pipe with BFC, the smaller the required amount of explosive charge to result in the buckling response of the pipe. The internal pressure of the pipe with BFC has the most significant influence on the conditions of the same pipe diameter and explosive. As a sequence, when determining the buried parameters of the high-pressurized pipes, the inner diameter of the pipe can be appropriately reduced under the premise of meeting the design requirements to improve the anti-explosion performance of the pipe.

6. Conclusions

In the present study, pipe-soil coupling 3-D models were established to investigate the dynamic buckling response of X70 steel pipe with BFC under two-charge explosion loads (Charge A lied on the ground surface and Charge B lied in the soil). The main influencing factors are also discussed, including explosion mode, internal pressure, interval time, mass ratio of charges, and diameter-to-thickness ratio (D/t ratio). The main obtained conclusions are as follows.

(1) When Charges A and B were exploded simultaneously, it is found that the non-pressurized X70 pipe produced more significant cross-sectional deformation than in one-point explosion (Charge A or B). When Charges A and B were exploded simultaneously, the flattening parameter value exceeds 0.6 and the pipe has significant deformation.

Table 8
List of the equation fitted for the data of orthogonal test.

	Equations	Correlation coefficient
1	$\sigma = 5.329(t)^{0.642}(P)^{0.221}(\sqrt[3]{Q})^{0.370}(R)^{0.070}$	0.910
2	$\sigma = 4.569(t)^{0.620}(P)^{0.189}(\sqrt[3]{Q})^{0.337}(R)^{0.061}$	0.975
3	$\sigma = 4.439(t)^{0.590}(P)^{0.203}(\sqrt[3]{Q})^{0.305}(R)^{0.055}$	0.851
4	$\sigma = 3.898(t)^{0.594}(P)^{0.165}(\sqrt[3]{Q})^{0.294}(R)^{0.053}$	0.898
5	$\sigma = 3.723(t)^{0.585}(P)^{0.158}(\sqrt[3]{Q})^{0.282}(R)^{0.051}$	0.899

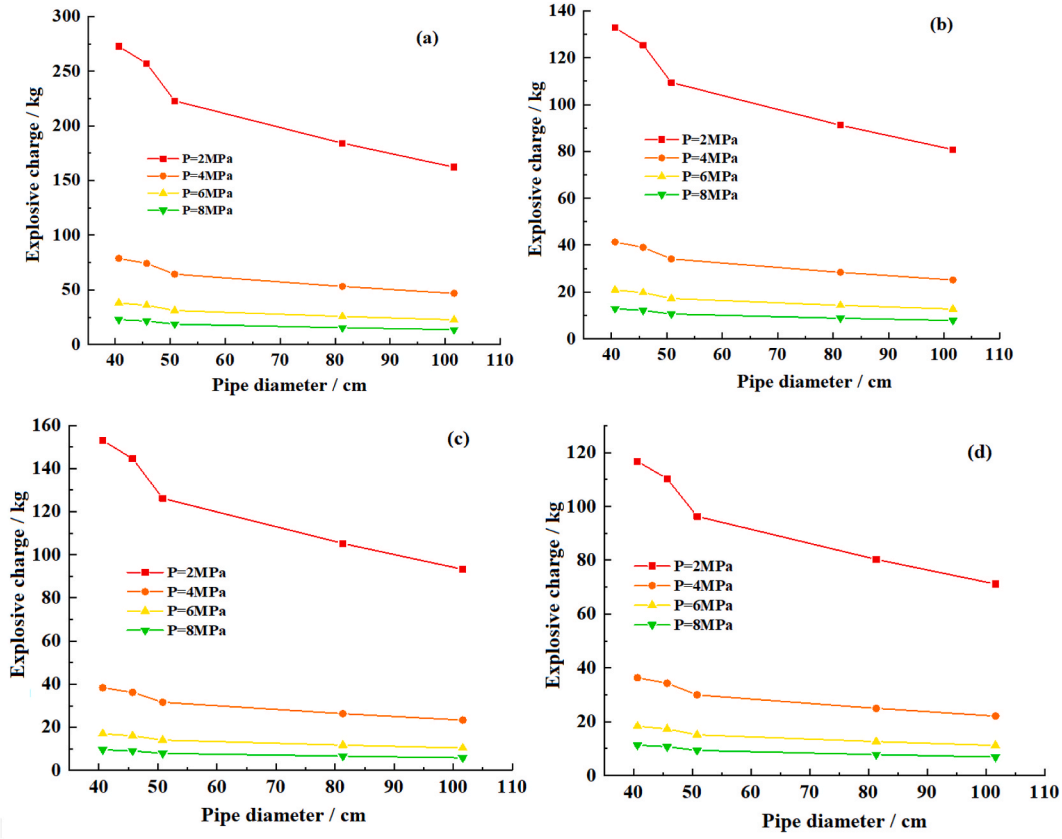

Fig. 15. The pipe diameter-explosive charge curves of the X70 pipe with BFC under two-charge explosion loads at different propagation times:(a) 300 μs; (b) 600 μs (c) 900 μs (d) 1200 μs.

(2) Internal pressure could effectively prevent the dynamic buckling deformation of the pipe under two-charge explosion loads. The non-pressurized pipe with BFC could obtain the peak plastic strain and the cross-sectional deformation reaches the maximum values. Designing the buried parameters of the pipe with higher pressure, the inner diameter of the pipe could be appropriately reduced under the premise of meeting the design requirements.
(3) The larger D/t ratio of the pipe is more susceptible to the damage of shock waves. Compared with the common straight pipes, the plastic strain of the pipe with BFC under the same two-charge explosion loads is smaller at the same interval time.
(4) Dimensional analysis of Golden Han Treatment was used to predict the stress of buried pipes under two-charge explosion loads and an approximate model was established to predict the peak stress of the pressurized X70 pipes with BFC under flat terrain condition.
(5) In order to reveal the buckling response mechanism of the X70 steel pipes with BFC under two-charge explosion loads, it is urgent to further carry out experimental study to obtain more experimental data.

Funding statement

This work was supported by Natural Science Foundation of China (Grant No. 52178461), National Science Foundation of Liaoning Province in China (Grand No. 2022-MS-165) and Scientific Research Foundation for Advanced Talents in Dalian Minzu University (Grant No.110233).

Data availability statement

Data associated with the study has not been deposited into a publicly available repository and data will be made available on request.

CRediT authorship contribution statement

Yandong Qu: Conceptualization, Supervision, Formal analysis, Investigation, Writing – Original Draft, Funding acquisition. **Ruixue Zhang:** Visualization, Software, Data Curation, Methodology, Formal analysis. **Jinda Wu:** Validation, Writing – Review &

Editing. **Lei Xu:** Formal analysis, Writing – Review & Editing. **Shengnan Zuo:** Writing – Review & Editing. **Baiyuan Xu:** Writing – Review & Editing.

Declaration of competing interest

The authors declare that they have no known competing financial interests or personal relationships that could have appeared to influence the work reported in this paper.

References

[1] L.P. Tang, W. He, H.X. Zhu, Y.L. Zhou, Mechanical analysis of un-bonded flexible pipe tensile armor under combined loads, Int. J. Pres. Ves. Pip. 171 (2019) 217–223, https://doi.org/10.1016/j.ijpvp.2019.02.015.

[2] Y.D. Qu, Z.P. Li, R.X. Zhang, Y.S. Qin, D.D. Zhang, Dynamic performance prediction and influencing factors analysis of buried polyethylene pipelines under subsurface localized explosion, Int. J. Press. Vessel. Pip. 189 (2021) 104252. https://doi:10.1016/j.ijpvp.2020.104252.

[3] C.S. Yang, S.Q. Li, Theoretical analysis and finite element simulation of pipeline structure in liquefied soil, Heliyon 7 (2021) E07480. https://doi:10.1016/j.heliyon.2021.e07480.

[4] X.M. Xiang, G. Lu, Z.X. Li, Y. Lv, Finite element analysis and experimental study on a bellows joint, Eng. Struct. 151 (2017) 584. https://doi:10.1016/j.engstruct.2017.08.034.

[5] I.R. Valiulin, E.A. Solovmev, A.S. Fik, O.Y. Elagina, N.N. Nikolaeva, Effect of welding technology on the mechanical properties of welded joints in pipes for deepwater offshore gas pipelines, Weld. Int. 31 (2017) 363, https://doi.org/10.1080/09507116.2016.1263457.

[6] X.M. Couchau, M. Hjiaj, I. Ryan, A. Bureau, Effect of contact on the elastic behavior of tensile bolted connections, J. Constr. Steel Res. 133 (2017) 459–474. https://doi:10.1016/j.jcsr.2016.10.012.

[7] M. Abid, N.B. Khan, Behavior of gasketed bolted pipe flange joint under combined internal pressure, axial, and bending load: three-dimensional numerical study, P I Mech Eng E-J PRO 232 (2018) 314, https://doi.org/10.1177/0954408917697888.

[8] V.L. Hoang, J.P. Jaspart, J.F. Demonceau, Behaviour of bolted flange joints in tubular structures under monotonic, repeated and fatigue loadings I: experimental tests, J. Constr. Steel Res. 85 (2013) 1, https://doi.org/10.1016/j.jcsr.2013.02.011.

[9] Y. Chen, C. Chen, B. Xue, W.J. Zhang, Y. Guo, J.Y. Wang, B.N. Sun, Experimental study of the bearing capacity of internal-external flange joints subjected to pressure and bending loadings with various eccentricities, Steel. Constr. 32 (2017) 16, https://doi.org/10.13206/j.gjg201703004 (In Chinese).

[10] C.F. Li, X.Y. Miao, R.H. Qiao, Q.S. Tang, Modeling method of bolted joints with micro-slip features and its application in flanged cylindrical shell, Thin Wall. Struct. 164 (2021) 107854, https://doi.org/10.1016/J.TWS.2021.107854.

[11] Y.H. Niu, B.M. Shi, B.Y. Jiang, Experimental study of overpressure evolution laws and flame propagation characteristics after methane explosion in transversal pipe networks, Appl. Therm. Eng. 154 (2019) 18, https://doi.org/10.1016/j.applthermaleng.2019.03.059.

[12] Y.D. Qu, Z.P. Li, J.Y. Li, D.L. Zou, R.X. Zhang, Y. Yu, Effect of weld geometry parameters on dynamic behavior of buried X70 steel pipeline under subsurface detonation, Int. J. Press. Vessel. Pip. 194 (A) (2021) 104504, https://doi.org/10.1016/J.IJPVP.2021.104504.

[13] K. Miltiadis, F. Clemente, Meta-material layout for the protection of buried steel pipes against surface explosion, Geotechnics 2 (2022) 427–440, https://doi.org/10.3390/GEOTECHNICS2020020.

[14] T.Y. Wu, N. Jiang, C.B. Zhou, X.D. Luo, H.B. Li, Y.Q. Xia, Dynamic response and safety assessment of buried gas pipe subjected to ground surface explosion, Int. J. Press. Vessel. Pip. 194 (A) (2021) 104527, https://doi.org/10.1016/J.IJPVP.2021.104527.

[15] M. Mokhtari, A.A. Nia, A parametric study on the mechanical performance of buried X65 steel pipelines under subsurface detonation, Arch. Civ. Mech. Eng. 15 (2015) 668, https://doi.org/10.1016/j.acme.2014.12.013.

[16] Y.H. He, Z.Y. Liu, Y.L. Ma, P. Cai, Z. Zuo, Numerical simulation study on the effect of large explosive contact pipeline explosion on pipeline damage, Thin Wall. Struct. 174 (2022) 109146, https://doi.org/10.1016/J.TWS.2022.109146.

[17] M. Parviz, B. Aminnejad, A. Fiouz, Numerical simulation of the dynamic response of water in the buried pipeline under explosion, KSCE. J. Eng. 21 (2017) 2798.

[18] Y.D. Qu, H.H. Yan, X.J. Li, H.-X. Liu, Overpressure Comparison of blasting in air and special-made hemispherical structure [J], Chin. J. High Press. Phys. 26 (1) (2012) 95–101. https://doi:10.11858/gywlxb.2012.01.014.

[19] Z.H. Liu, O.T. Gudmestad, R. Igland, Numerical simulation of a subsea pipeline subjected to underwater explosion loads with the coupled Eulerian-Lagrangian (CEL) method, J. Offshore Mech. Arct. Eng 144 (2022) 061901, https://doi.org/10.1115/1.4054830.

[20] Y. Lu, Y. Ding, J.H. Zhang, M. Yang, Study on the calculation method and structural dynamic response of buried pipeline subjected to external explosion load based on multiphase coupling, Heliyon 9 (2023) E18549, https://doi.org/10.1016/J.HELIYON.2023.E18549.

[21] J. Zhang, H. Zhang, L. Zhang, L. Zheng, Buckling response analysis of buried steel pipe under multiple explosive loadings, J. Pipeline. Syst. Eng. 11 (2020) 04020010, https://doi.org/10.1061/(ASCE)PS.1949-1204.0000431.

[22] K. Zhao, N. Jiang, Y.S. Jia, Y.K. Yao, B. Zhu, C.B. Zhou, Dynamic failure mechanism of gas pipeline with flange joint under blasting seismic wave, Explosive and Shock Waves 41 (2021) 095101, https://doi.org/10.11883/bzycj-2020-0320.

[23] C. Ji, F.Y. Gao, X.H. Li, Y. Yu, L.Y. Cheng, Numerical analysis of vibration-isolating effect of vibration-isolating slot under buried pipe subjected to millisecond blasting, Vibroengineering Procedia 21 (2018) 32, https://doi.org/10.21595/vp.2018.20213.

[24] Z.T. An, Q. Tang, Y.F. Huang, H. Li, Time-dependent analysis of buried high-density polyethylene (PE100) pipelines with a scratch defect subjected to touchdown impact loading of blasting collapsed body, Int. J. Press. Vessel. Pip. 195 (2022) 104605, https://doi.org/10.1016/J.IJPVP.2021.104605.

[25] E. Govahi, M. Salkhordeh, M. Mirtaheri, Cyclic performance of different mitigation strategies proposed for segmental precast bridge piers, Structures (36) (2022) 344, https://doi.org/10.1016/J.ISTRUC.2021.12.020.

[26] M. Lee, H.-G. Kwak, Numerical simulations of blast responses for SFRC slabs using an orthotropic model, Eng. Struct. 238 (2021) 112150, https://doi.org/10.1016/J.ENGSTRUCT.2021.112150.

[27] W.J. Zhang, X.Q. Kong, Y.D. Qu, Q. Zhao, Numerical simulation of cracked reinforced concrete slabs subjected to blast loading, Civ. Eng. J. 4 (2018) 320, https://doi.org/10.28991/cej-030994.

[28] Y.D. Qu, W.L. Liu, M. Gwarzo, W.J. Zhang, C. Zhai, X.Q. Kong, Parametric study of anti-explosion performance of reinforced concrete T-shaped beam strengthened with steel plates, Constr. Build. Mater. 156 (2017) 692, https://doi.org/10.1016/j.conbuildmat.2017.08.150.

[29] R. Hájek, K. Horníková, M. Foglar, Numerical assessment of the response of a heterogeneous concrete-based composite bridge deck to a near field explosion, Eng. Struct. 225 (2020) 111206, https://doi.org/10.1016/j.engstruct.2020.111206.

[30] Z.P. Li, Y.D. Qu, Dynamic response analysis of buried X70 steel pipe near weld zone under blast loads, Chin. J. High Press. Phys. 34 (2020) 034204, https://doi.org/10.11858/gywlxb.20190831.

[31] K.J. Song, Y. Long, C. Ji, F.Y. Gao, H.L. Chen, Experimental and numerical studies on the deformation and tearing of X70 pipelines subjected to localized blast loading, Thin Wall. Struct. 107 (2016) 156, https://doi.org/10.1016/j.tws.2016.03.010.

[32] T.T. Wang, A.S. Cao, W.L. Gao, G.Y. Wang, X.W. Sun, Damage evolution and circumferential strain distribution characteristics of the bolt-supported cavern under multiple explosion sources, Shock Vib. (2021) 9985774, https://doi.org/10.1155/2021/9985774, 2021.

[33] T.T. Wang, A.S. Cao, Z. Dun, L. Ren, X. Sun, Numerical simulation of the dynamic responses and cumulative damage of underground caverns under multiple explosions, Shock Vib. (2020) 8836375, 2020.

[34] G.Y. Wang, A.S. Cao, X.Y. Wang, R. Yu, X. Huang, J.J. Lin, Numerical simulation of the dynamic responses and damage of underground cavern under multiple explosion sources, Eng. Fail. Anal. 120 (2021) 105085, https://doi.org/10.1016/j.engfailanal.2020.105085.
[35] F. Bai, Y. Liu, J.B. Yan, Y.L. Xu, Z.Q. Shi, F.L. Huang, Study on the characteristics of blast loads due to two simultaneous detonated charges in real air, Int. J. Non Lin. Mech. 146 (2022) 104108, https://doi.org/10.1016/j.ijnonlinmec.2022.104108.
[36] X.Y. Huang, X.P. Hu, L. Zhang, Z.H. Cai, Craniocerebral dynamic response and cumulative effect of damage under repetitive blast, Ann. Biomed. Eng. 49 (2021) 1, https://doi.org/10.1007/s10439-021-02746-7, 2021.
[37] A.S. Fallah, E. Nwankwo, L.A. Louca, Pressure-impulse diagrams for blast loaded continuous beams based on dimensional analysis, J. Appl. Mech. 80 (2013) 051011, https://doi.org/10.1115/1.4023639.
[38] J.J. Shi, S.C. Guo, W. Zhang, Expansion of blast vibration attenuation equations for deeply buried small clearance tunnels based on dimensional analysis, Front. Earth Sci. 10 (2022) 889504, https://doi.org/10.3389/feart.2022.889504.
[39] Y.D. Qu, J.D. Wu, B.Y. Xu, Q.Y. Li, Evaluating the shape and orientation effect of non-spherical charge on the pressure distribution of underwater explosion: finite element analysis, Ocean Eng 266 (2022) 113209, https://doi.org/10.1016/j.oceaneng.2022.113209.
[40] R. Castedo, M. Natale, L.M. Lopze, J.A. Sanchidrián, A.P. Santos, J. Navarro, P. Segarra, Estimation of Jones-Wilkins-Lee parameters of emulsion explosives using cylinder tests and their numerical validation, Int. J. Rock Mech. Min. Sci. 112 (2018) 290–301, https://doi.org/10.1016/j.ijrmms.2018.10.027.
[41] A. Maazoun, S. Matthys, B. Belkassem, D. Lecompte, J. Vantomme, Blast response of retrofitted reinforced concrete hollow core slabs under a close distance explosion, Eng. Struct. 191 (2019) 447–459, https://doi.org/10.1016/j.engstruct.2019.04.068.
[42] C.H. Li, L.Y. Wei, C.W. Chang, Experiment piping numerical simulation of explosion compaction in loess, Explosive and Shock Waves 38 (2018) 289, https://doi.org/10.11883/byzcj-2016-0251.
[43] R.L. Chen, Q. Dong, Numerical simulation for dynamic responses of flange connection structures under blast impact loads, J. Vib. Shock 37 (2018) 56, https://doi.org/10.13465/j.cnki.jvs.2018.17.008.
[44] Ls-Dyna, Keyword User's Manual. Version 970, Livemore Software Technology Corporation (LSTC), Livermore, 2006.
[45] GB/T 34275—2017, Pressure Piping Code-Long-Distance Pipelines, Standards Press of China, Beijing, China, 2017.
[46] GB/T 9124.1-2019, Steel Pipe Flanges—Part 1 : PN Designated, Standards Press of China, Beijing, China, 2019, 12-01.
[47] K. Wang, Z.Y. Liu, X.M. Qian, Y.R. He, Dynamic characteristics and damage recognition of blast-induced ground vibration for natural gas transmission pipeline and its integrated systems, Mech. Syst. Signal Process. 136 (2020) 106472, https://doi.org/10.1016/j.ymssp.2019.106472.
[48] Y.D. Qu, X. Li, X.Q. Kong, W.J. Zhang, X.Z. Wang, Numerical simulation on dynamic behavior of reinforced concrete beam with initial cracks subjected to air blast loading, Eng. Struct. 128 (2016) 96, https://doi.org/10.1016/j.engstruct.2016.09.032.
[49] A.M. Gresnigt, Plastic design of buried steel pipes in settlement areas, Heron 31 (1986) 1–113.